Simulation of Electron Streamline Distribution in the Coupling Area of Hall Thruster

IEPC-2017-155

Presented at the 35th International Electric Propulsion Conference
Georgia Institute of Technology • Atlanta, Georgia • USA
October 8 – 12, 2017

Tianhang Meng[1], Zhongxi Ning[2] and Daren Yu[3]
Harbin Institute of Technology, Harbin, Heilongjiang, 150001, China

Abstract: This article built a double-ion-fluid model in COMSOL to simulate the electron streamline distribution in the coupling area of a Hall thruster. Virtual cathode, the dense electron beam emitting from cathode orifice and curling along magnetic field, was noticed to dominate the global flow. The dependence of virtual cathode on cathode location, vacuum backpressure and tank walls was then investigated. Results show that when changing these three factors, the virtual cathode can relocate by rotating over 270° and subsequently changing the coupling voltage significantly. Considering the close connection between coupling voltage with plume divergence, ground-orbit inconsistency, in-orbit communication interference and solar panel erosion, bending the virtual cathode towards the ion beam might be a more favorable design. We also appeal attention to the undesirable influence of auxiliary equipment on virtual cathode during experiments.

Nomenclature

n_e	=	electron density
$\boldsymbol{\Gamma_e}$	=	electron flux density
t	=	time
R_e	=	reaction source term
$\boldsymbol{u}$	=	flow velocity
$\boldsymbol{\mu_e}$	=	electron mobility tensor
$\boldsymbol{E}$	=	electric field intensity
$\boldsymbol{F_{ie}}$	=	equivalent friction force of beam ions on electrons
$\boldsymbol{D_e}$	=	electron diffusivity tensor
v_{ie}	=	ion-electron Coulomb collision frequency
$\boldsymbol{V_i}$	=	ion flow velocity
B_α	=	magnetic field intensity in each coordinate
v_{ea}	=	electron-atom collision frequency
n_ε	=	electron energy density
S_{en}	=	energy loss due to collisions
Q	=	external heat source
Q_{gen}	=	generalized heat source
q	=	unit charge
$\boldsymbol{\mu_{en}}$	=	electron energy mobility tensor
$\boldsymbol{D_{en}}$	=	electron energy diffusivity tensor

[1] Doctoral Student, School of Energy Science and Engineering, mengtianhang1989@163.com
[2] Associate Professor, School of Energy Science and Engineering,, ningzx@hit.edu.cn
[3] Professor, School of Energy Science and Engineering,, yudaren@hit.edu.cn

v_{ii} = ion-ion collision frequency
Kn_{ii} = ion Knudsen number due to ion-ion collisions
n_i = ion density
$ln\Lambda$ = Coulomb logarithm
μ = relative atom mass
T_i = ion temperature
Z_i = ion charge number
λ_{ii} = ion mean free path due to ion-ion collisions
R = characteristic spatial length
$v_{th,i}$ = ion thermal velocity
ρ = heavy particle density
w = heavy species mass fraction
R_i = reaction source term
j_i = heavy particle flux density
$\boldsymbol{V_d}$ = velocity averaged over all heavy species
D_i^m = average diffusivity coefficient
M_n = average molar mass
D_i^T = thermal diffusivity coefficient of each heavy species
T = gas temperature
μ_m = average mobility
k = Boltzmann constant
m_i = ion mass
Ma_i = ion Mach number
T_e = electron temperature
k^f = reaction frequency
c_k = concentration of each reaction participant
P = neutral pressure
$\boldsymbol{r}$ = Euler distance
E_r = radial electric field intensity
r_c = radial location of cathode orifice

I. Introduction

THE core technology of Hall thrusters is the flow control of electrons. Increasing evidence indicates that the electron flow outside the acceleration channel, especially in the 'coupling area', disturbs the physical processes inside the channel and affects overall performance output.[1-5] However, lacking attention to this 'exhaust region' in the past, the physical images of outside flow and coupling are quite fuzzy.[6] To avoid guessing in analysis, data on all levels are seriously needed.

There has been indeed experimental data of the coupling area, including density, temperature and potential distribution, under many researchers' efforts.[7-14] However, deriving a flow field from these data requires appropriate physics models. With anomalous transport haunting, there is quite uncertainty in the coefficients. On the other hand, using specific probe techniques to measure flow field directly may face practical difficulties. Due to the zoo of instabilities inhabiting the plume, the signal-to-noise ratio can hardly be enough for such subtle measurements. Also, sophisticated magnetic and thermal correction need be considered due to the ion beam sputtering, strong magnetic field and low plasma density in this area. Therefore, gaining flow information through diagnostics is very challenging.

Naturally, one may resort to numerical simulation. Due to large spatial scales of outside field, and that the backpressure in coupling area is on the magnitude of Pascal, the Knudsen number of ions is estimated to be less than 0.01, which is in continuum region. On the other hand, the scales of electrons' motion are even smaller than ions'. Therefore, for the case of static coupling with both large spatial and time scale, fluid description is legal,[15-17] sometimes also efficient.

Furthermore, previous fluid simulations used to concentrate on the near field after channel exit. Recent experiments found that some ignored areas, including the flank area and the far field, also participate in coupling.[18,19] Obtaining the new images in such areas may help refresh our understanding of coupling, even the global Hall discharge.

Motivated by these thoughts, we modified the Extended Fluid Model in COMSOL to gain flow information, especially the electron streamlines of the coupling area. After that we investigated the influence of hollow cathode location, vacuum backpressure and tank walls. Section II will describe the equations and settings. Section III will discuss the characteristics of the virtual cathode among normal electron streamlines. Section IV gives conclusions and future plans.

II. Model Description

The general guideline of Extended Fluid Model in COMSOL is as follows. For electrons, the energy flow and mass flow are assumed to share the same orientation, so the continuity equation and energy conservation equation are solved in pairs to give electron velocities. As for heavy particles, Fick's law determines cross-phase diffusion and ion velocities. The reaction terms in electron and ion equations are from collisions. The electric field is solved in Poisson Equation.

A. Electron Equations

Continuity equation for electrons is:

$$\frac{\partial n_e}{\partial t} + \nabla \cdot \boldsymbol{\Gamma_e} = R_e - \boldsymbol{u} \cdot \nabla \mathrm{n}_e \tag{1}$$

, in which n_e is electron density, $\boldsymbol{\Gamma_e}$ electron flux density, R_e the reaction source term and $\boldsymbol{u}$ the flow velocity.

Electron flux density $\boldsymbol{\Gamma_e}$ is:

$$\boldsymbol{\Gamma_e} = -(\boldsymbol{\mu_e} \cdot \boldsymbol{E} + \boldsymbol{F_{ie}})n_e - \boldsymbol{D_e} \cdot \nabla n_e \tag{2}$$

, in which $\boldsymbol{\mu_e}$ is the mobility tensor, $\boldsymbol{E}$ electric field intensity and $\boldsymbol{D_e}$ diffusion coefficient. $\boldsymbol{F_{ie}}$ is the equivalent friction force of beam ions on electrons. Due to the high energy transfer efficiency during ion-electron collision, the beam ions are assumed to give all their flow velocity to electrons in each collision. Then the equivalent friction is:

$$\boldsymbol{F_{ie}} = v_{ie} m_e \boldsymbol{V_i} \tag{3}$$

, in which v_{ie} is ion-electron collision frequency, $\boldsymbol{V_i}$ is ion flow velocity.

Mobility and diffusivity are in tensors and assumed to obey Einstein's Relation:

$$\mu_{e,\alpha\beta} = \frac{A}{\frac{1}{\mu_e^3} + \frac{|\boldsymbol{B}|^2}{\mu_e}} \quad , \qquad A = \begin{cases} \frac{1}{\mu_e^2} + B_\alpha^2, & \alpha = \beta \\ B_\alpha B_\beta \pm \frac{B_\gamma^2}{\mu_e^2}, & \alpha \neq \beta \end{cases} \tag{4}$$

, in which $\mu_e = e/mv_{ea}$, temporarily only electron-atom collisions are considered. B_α is magnetic field strength in each coordinate. In this article we used the cylindrical coordinates.

Energy conservation equations for electrons is:

$$\frac{\partial n_\varepsilon}{\partial t} + \nabla \cdot \boldsymbol{\Gamma_\varepsilon} + E \cdot \boldsymbol{\Gamma_e} = S_{en} - \boldsymbol{u} \cdot \nabla n_\varepsilon + \frac{Q + Q_{gen}}{q} \tag{5}$$

, in which n_ε is energy density and S_{en} the energy loss due to collisions.

Energy flux density Γ_ε is:

$$\Gamma_\varepsilon = -\left(\boldsymbol{\mu_{en}} \cdot \boldsymbol{E} + \frac{\boldsymbol{5F_{ie}}}{\boldsymbol{3}m_e v_{ea}}\right) n_\varepsilon - \boldsymbol{D_{en}} \cdot \nabla n_\varepsilon \tag{6}$$

, in which $\boldsymbol{\mu_{en}}$ is energy mobility tensor $\boldsymbol{\mu_{en}} = \frac{5}{3}\boldsymbol{\mu_e}$ and $\boldsymbol{D_{en}}$ the energy diffusivity coefficient. v_{ea} is electron-atom collision frequency.

B. Heavy Particle Transport

When the thermal energy of ions is less than 50eV, the ion-ion collision frequency is:

$$v_{ii} = 4.8 \times 10^{-8} Z_i^4 \frac{n_i ln\Lambda}{\sqrt{\mu} T_i^{1.5}} \approx 1MHz \tag{7}$$

, in which v_{ii} is ion-ion collision frequency, Z_i the charge number of ions, n_i the ion density, $ln\Lambda$ the Coulomb logarithm, μ relative atom mass, and T_i the ion temperature.

Then the Knudsen number of ions is:

$$\mathrm{Kn}_{ii} = \frac{\lambda_{ii}}{R} = \frac{v_{th,i}}{v_{ii} R} < 1.5 \times 10^{-3} \tag{8}$$

, which is in continuum region. The Knudsen number of atoms is estimated to be 0.1~1, which is in transitional region. Then the continuity of each phase of heavy particles is:

$$\rho \frac{\partial w}{\partial t} + (\boldsymbol{u} \cdot \nabla) w = R_i - \nabla \cdot \boldsymbol{j_i} \tag{9}$$

, in which ρ is heavy particle density, *w* the mass fraction, R_i the reaction source term and $\boldsymbol{j_i}$ the flux density.

Flux density $\boldsymbol{j_i}$ is:

$$\boldsymbol{j_i} = \rho w \boldsymbol{V_d} = \rho w (D_i^m \nabla ln w + D_i^m \nabla ln M_n + \frac{D_i^T}{\rho w} \nabla ln T - z_i \mu_m \boldsymbol{E}) \tag{10}$$

, in which $\boldsymbol{V_d}$ is velocity averaged over all species, D_i^m average diffusivity coefficient, M_n average molar mass, D_i^T thermal diffusivity coefficient of each phase, T gas temperature, and μ_m average mobility.

Please notice that when there are supersonic ion flow injected to a plasma, above equations need a further check, or they may create false jamming and convections. The thermal velocity of ions is:

$$\mathrm{v}_{th,i} = \sqrt{\frac{8kT_i}{\pi m_i}} \approx 900\mathrm{m/s} \tag{11}$$

, assuming the specific impulse is 2000s, then the ion Mach number $\mathrm{Ma}_i > 20$. Even if Bohm speed is adopted:

$$\mathrm{v}_{th,i} = \sqrt{\frac{kT_e}{m_i}} \approx 2.7\mathrm{km/s} \tag{12}$$

, still ion Mach number $\mathrm{Ma}_i > 7$. This will create jamming easily between upstream and downstream elements, if the electron or ion temperature is incorrect. On the other hand, due to the Coulomb collision between beam ions (300eV) and slow ions (5eV), the 'Knudsen number' between them is:

$$\mathrm{Kn}'_{ii} = \frac{\lambda'_{ii}}{R} = \frac{v_{th,i}}{v'_{ii} R} \approx 0.2 \tag{13}$$

, which is in transitional region. So as beam ions are significantly faster than slow ions, there isn't strong convection between them. The false jamming and convection usually lead to convergence failure. Inspired by Ref.16, this article distinguished these two ions. The first species, the beam ions bXe^+, are injected from the inlet boundary and allowed only to recombine or CEX collide with neutrals irreversibly. They are not allowed to rejuvenate from ionization. On the contrary, the second species, the slow ions Xe^+, are born inside the domain without specific impulse. They come from ionization or CEX collisions. Section III will show their difference.

C. Reactions

All reaction terms come in form of:

$$r = k^f \prod c_k \tag{14}$$

, in which *r* is source term R_e or R_i, k^f reaction frequency, c_k concentration of each participant.

The reactions included are given in Table 1, and the cross section data is from Lxcat database.[20]

Table 1 Plasma reactions

Reaction Formula	Category
e+Xe=>e+Xe	Elastic collision
e+Xe=>e+e+Xe$^+$	Direct ionization
e+Xe<=>e+Xe01/Xe02/Xe03	Excitation and de-excitation of ground state
e+Xe01/Xe02<=>e+Xe02/Xe03	Excitation and de-excitation of metastable atoms
e+Xe01/Xe02/Xe03=>e+e+Xe$^+$	Ionization of metastable atoms
Xe03/Xe02/Xe01=>Xe	Radiation de-excitation
Xe03/Xe02+Xe=>Xe02/Xe01+Xe	Metastable quenching
Xe01/Xe02+Xe01/Xe02=>e+Xe+Xe$^+$	Penning ionization
e+Xe$^+$=>Xe	Radiative recombination
e+e+Xe$^+$=>e+Xe	Collisional recombination
bXe$^+$/Xe$^+$+Xe=>Xe+Xe$^+$	Charge exchange (CEX) collision

D. Boundary and Initial Conditions

The benchmark experimental data borrowed in this work is from a Hall thruster with 85mm outer wall diameter. Its anode mass flow rate is 44sccm and cathode 3sccm. In operation, the anode voltage is 400V and anode current 4A. The vacuum tank is 1.2m in diameter and 3m long. The vacuum is 1×10^{-2}Pa during discharge.

Correspondingly, the calculation domain is a 0.6m×1m axisymmetric region. Its boundary conditions are shown in Figure 1. The hall thruster is the blank box in the middle. Its edges are set floating and electron-reflective. The cathode is compromised as an axisymmetric ring, emitting electrons with 2eV initial temperature. The upmost edge facing the plume is a disappearance outlet for both electrons and heavy particles. To simulate the tank walls, flank and rear boundaries are grounded and absorbing electrons. Temporarily Maxwellian EEDF is used.

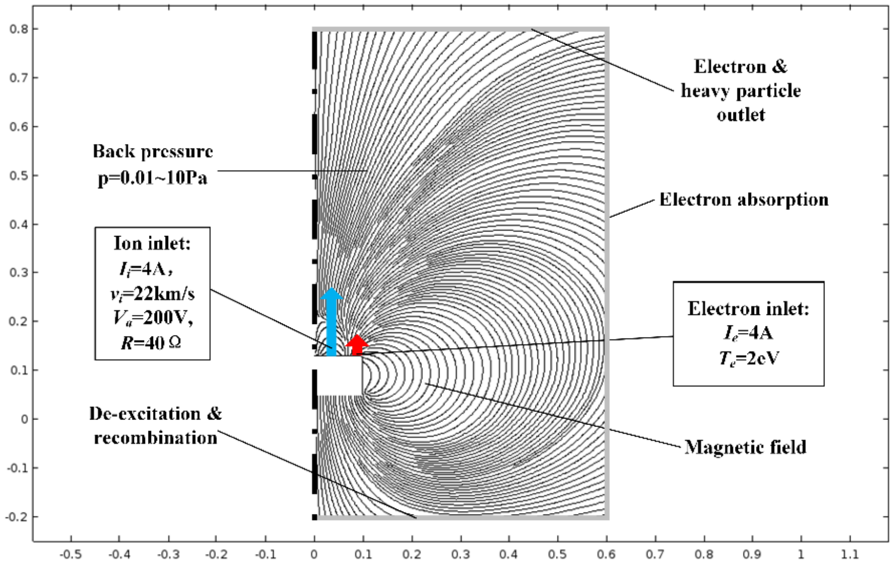

Figure 1. Boundary condition of simulation

4A beam ions are injected from thruster upper edge with 22km/s initial velocity. After that the ions can de-excite or recombine on the flank and rear boundaries. The vacuum backpressure obeys free molecular flows, ranging from 10Pa at thruster exit to 0.01Pa at the most distant point:

$$P = P_1 + P_2 + P_3$$
$$P_1 = \frac{0.5}{99|(\boldsymbol{r}-\boldsymbol{r_1})^2|+0.1},\ P_2 = \frac{0.5}{99|(\boldsymbol{r}-\boldsymbol{r_2})^2|+0.1},\ P_3 = \frac{1}{99|(\boldsymbol{r}-\boldsymbol{r_3})^2|+0.1} \quad (15)$$

The magnetic field are calculated by FEMM and imported into COMSOL. The magnetic field strength is about 250Gs at channel exit, and over 3000Gs on axis. The segment representing the channel exit has a 200V potential with respect to cathode and ground, and a 40Ω ballast resistor in series so that the coupling voltage can self-adjust.

The initial electron temperature is 6eV, plasma density $1\times10^{16}/m^3$ and potential 50V. To ensure static distribution, the time length is 100s.

III. Results and Discussion

A. Model Validation

Figure 2 and Figure 3 show the electron density and temperature distribution in the coupling area. Because the thruster is operating in high-specific-impulse mode, the electron density at thruster exit is as low as $5\times10^{16}/m^3$. The electron temperature is 2~9eV (not including kinetic energy), agreeing with other references.[7-9] It can be clearly seen that with 3000Gs on central axis, a high density line formed. This agrees with visual observations. A green glowing line can be seen at the same location during experiments.

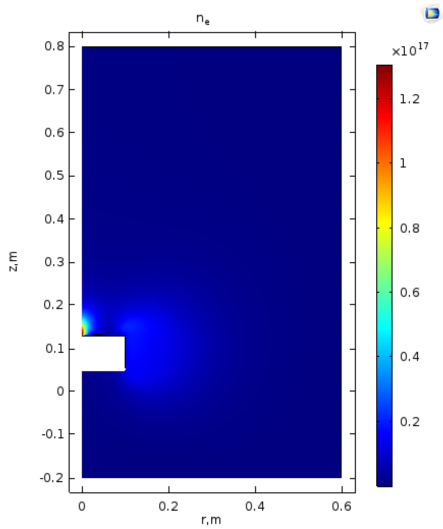

Figure 2. Electron density distribution in coupling area

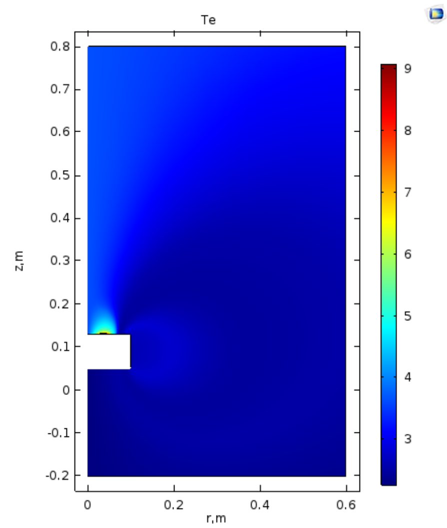

Figure 3. Electron temperature distribution in coupling area

The potential difference between channel exit and the cathode is called coupling voltage. It is an important indicator of coupling process, thus a concerned benchmark parameter in our work. As Figure 4 shows, the computed coupling voltage is 48V, within the acceptable range of 30~60V. [7-9] Radial distribution at different axial locations are show in Figure 5. During fixing these distributions, we found that although coupling was generally about the near field, the distant tank walls need to be obtained. Only when the flank and rear boundaries are grounded, could computed plume potential be as high as experimental results. Otherwise, such as setting these boundaries as floating and/or heavy particle outlets, the computed potential can be one magnitude lower than experiment results, meanwhile the voltage between plume axis and plume edge can be two magnitude lower (Figure 5).

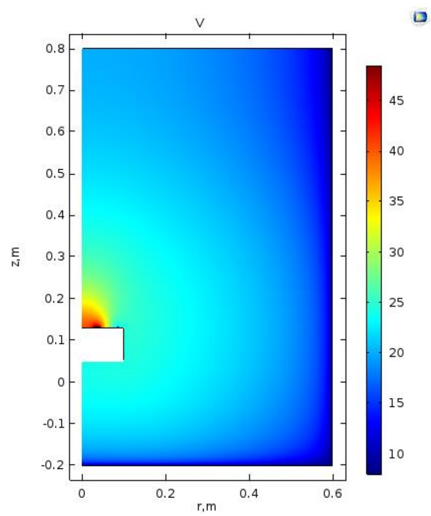

Figure 4. Space potential distribution in coupling area

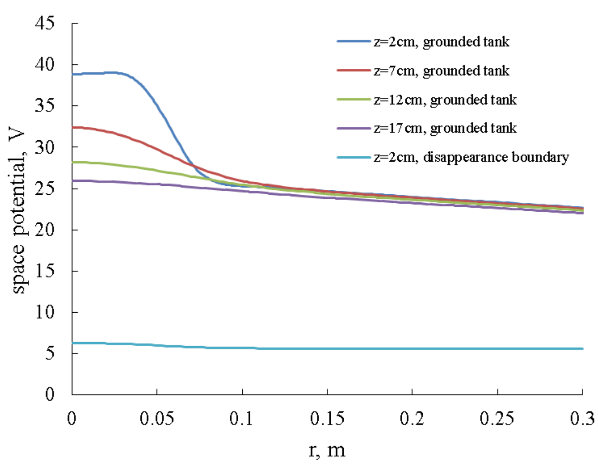

Figure 5. Radial distribution of space potential at different axial locations away from thruster exit

B. Virtual Cathode Characteristics

After improving electric field accuracy in distant areas, we mapped the global electron streamline distribution. A cluster of streamlines threading the cathode orifice caught our attention. They have higher electron density and lower electron temperature and potential, usually curling along local magnetic field. By coincidence, in most cases they coincide with the 'red glow' enclosing the thruster body seen in the experiments. This confirms that the 'red glow' is actually the result of dense electrons trapped in the outer magnetic mirrors and exciting neutrals. Mimicking the definition in cathode electronics, we temporarily name this cluster of dense electrons as the 'virtual cathode'. We assume that other streamlines are just tributaries of the virtual cathode.

Dependence investigation shows that the virtual cathode is very sensitive to barriers (tank walls), cathode location and vacuum backpressure. Figure 6 shows the virtual cathodes during expanding the domain. It is obvious that boundaries bend the direction of virtual cathode. As the boundary retreats from thruster exit plane to rear space, the virtual cathode 'grows' towards the thruster backplate. Playing back this process, if a certain barrier blocking this growth approaches the ion beam, the virtual cathode will bend towards the ion beam. In the examples in Figure 6, the bending direction of the virtual cathode turned by about 90°.

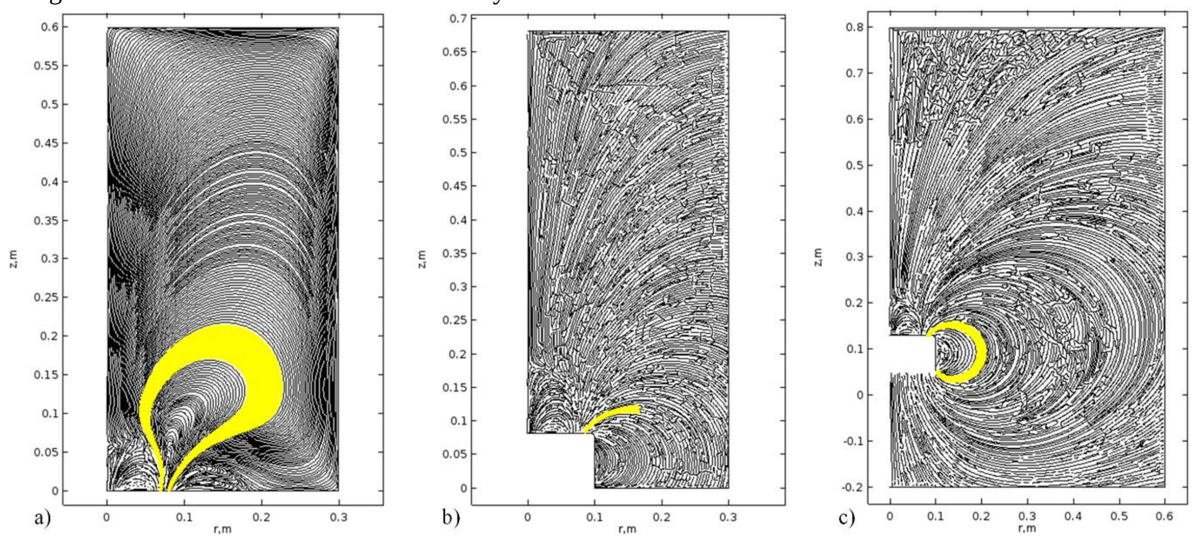

Figure 6. Virtual cathodes during expanding simulation domain

a) no flank or rear space, b) obtained flank space, c) further obtained rear space

As the virtual cathode emits from cathode orifice, it is certainly influenced by cathode location. Figure 7 compares the cases with different cathode locations. The cathode was moved radially towards the central axis across the magnetic separatrix. Before and after the crossing, the magnetic field line threading the cathode orifice changed its end point from the backplate first to infinitely remote point, then from infinity to the front face of inner magnetic pole. Following the magnetic line, the virtual cathode rotated by nearly 270°, although the cathode moved by only 2cm. This flipping movement of virtual cathode agrees with visual observations in experiments.[19]

Considering that the virtual cathode could extend to low pressure area, we also investigated the influence of vacuum backpressure. Figure 8 shows the cases with backpressure ranging from 6×10^{-3}Pa to 1.3×10^{-1}Pa. Background neutrals help transport electrons in transverse magnetic field direction, so under higher backpressure, the virtual cathode can more easily escape magnetization and flow to high potential areas, as shown in Figure a). On the other hand, when the virtual cathode is highly magnetized in high vacuum condition, the flanking plasma bulk will receive more environment factors into Hall discharge, such as space plasma interference. This might partly explain the performance discrepancies in different vacuum conditions.

C. Consequences of Virtual Cathode Relocation

One known consequence of virtual cathode relocation is the re-adjusting of coupling voltage. Figure 9 a) shows the computed radial potential distribution under different backpressure. The data was chosen at 40mm downstream thruster exit. Recalling Figure 6, when the backpressure increases, the virtual cathode relocated from flank area to the ion beam. This will reduce the coupling voltage because a) the electrons would have to traverse less magnetic field lines and b) less charge separation reduces local electric field. In Figure 9 a) the coupling voltage dropped by 60V (79%).

Responding to the re-distribution of electric field, the ion trajectories will also change. Figure 9 b) shows the ion streamlines for both beam ions and slow ions. As can be seen, both species will deviate radially in radial electric field $\boldsymbol{E_r}$, causing plume divergence. But the slow ions deviate more because they have longer dwelling time in the domain. It is expected that with lower coupling voltage and thus weaker $\boldsymbol{E_r}$, the plume can be much more focused. Especially for the CEX ions, as they are even slower than slow ions, their divergence might be greatly suppressed.

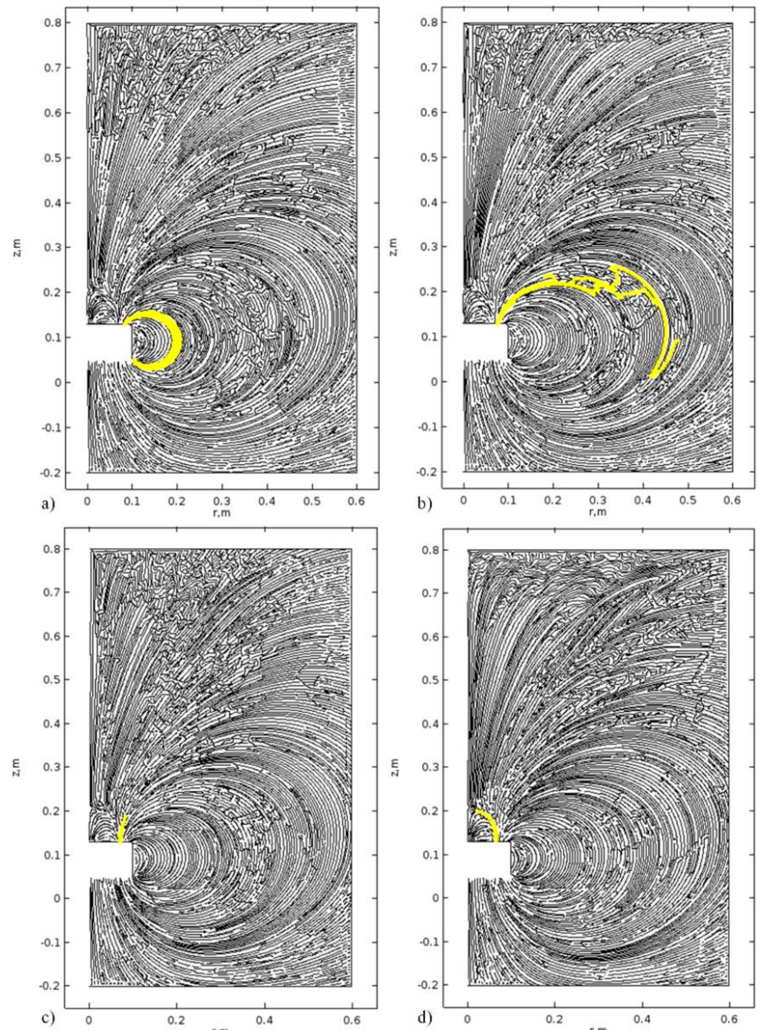

Figure 7. Virtual cathodes with different cathode locations
a) r_c=85mm, b) r_c=77mm, c) r_c=70mm, d) r_c=65mm

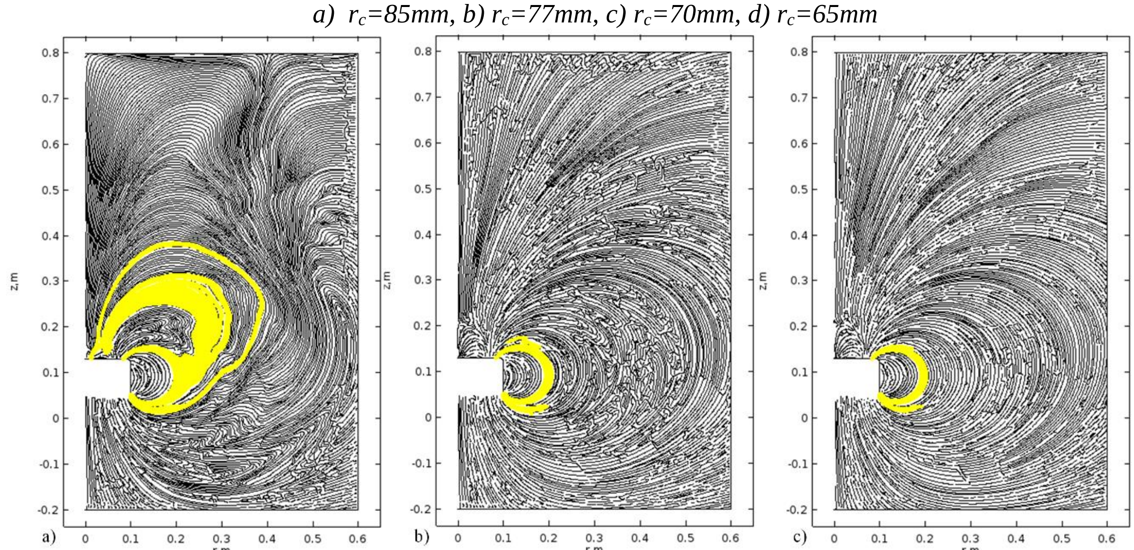

Figure 8. Virtual cathodes under different vacuum backpressure
a) $p=1.3\times10^{-1}Pa$, b) $p=1.2\times10^{-2}Pa$, c) $p=6\times10^{-3}Pa$

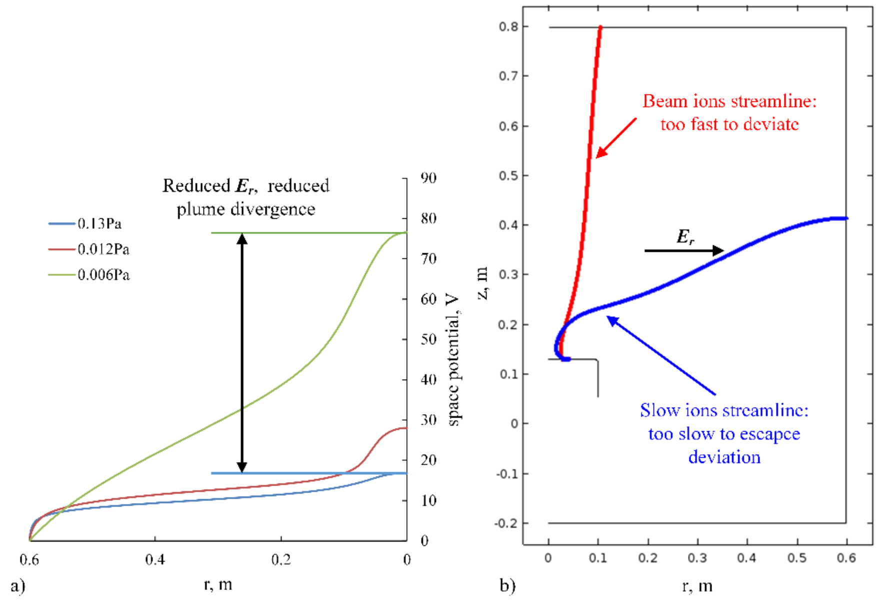

Figure 9. Connection between backpressure, coupling voltage and plume divergence

So there is connection between the virtual cathode, outer electric field and ion beam behaviors. From engineering perspective, this can be beneficial. If tuning the virtual cathode can reduce coupling voltage by 60V, then the voltage efficiency would increase from 68.5% to 83.5%, together with higher mass utilization efficiency and higher thrust output. In addition, a less divergent plume will increase plume angle efficiency, reduce CEX ions sputtering and ease communication interference in the far field.

IV. Conclusion

This article modified the Extended Fluid Model in COMSOL into double-ion-fluid model to investigate the influence of tank walls, vacuum backpressure and cathode locations on the electron streamline distribution in Hall thruster coupling area, especially on the virtual cathode within. Results show that changing these factors will cause the virtual cathode relocation (in our cases rotation by a large angle), thus impacting outer electric field distribution and ion trajectories consequently. Considering that designs with flanking virtual cathode may face problems of low voltage efficiency, large plume divergence angle, more ground-orbit discrepancies, higher CEX sputtering rate and stronger communication interference, bending the virtual cathode towards the ion beam might be a more favorable design. In addition, considering that the auxiliary equipment inside the vacuum tank, including the frames and installation plates could severely twist the direction of virtual cathode thus bring in ground-orbit discrepancies, perhaps the experiments should try to shrink the size of these equipment, especially the plate carrying the thruster.

The model in this paper is in engineering-phase. In the future, more physics have to be considered in the transport coefficients and wall models. Also, some frequencies recently found in the coupling oscillations suggest digging in the transient modeling.

Acknowledgments

The first author would like to thank Dr. Stepan Eliseev for the software assistance and Prof. Anatoly A. Kudryavtsev for the enlightening discussion. This work was supported by the Special Subsidy of China-Russia Personnel Exchange and Research Cooperation Base of Harbin Institute of Technology.

References

[1] Tilley, D., de Grys, K., Myers, R., "Hall Thruster-cathode Coupling," *35th Joint Propulsion Conference and Exhibit*, AIAA, 1999.

[2] McDonald, M. S., Gallimore, A. D., "Cathode Position and Orientation Effects on Cathode Coupling in a 6-Kw Hall Thruster," *31st International Electric Propulsion Conference*, 2009.

[3] Carpenter C., "Comparison of On-Orbit and Ground Based Hollow Cathode Operation," *38th AIAA/ASME/SAE/ASEE Joint Propulsion Conference & Exhibit*, NASA, 2002.

[4] Beal B. E. and Gallimore A. D., "Effects of Cathode Configuration on Hall Thruster Cluster Plume Properties," *Journal of Propulsion and Power*, Vol.23, No.4, 2007, pp: 836, 844.

[5] Sommerville, J. D., King, L B., "Effect of Cathode Position on Hall-Effect Thruster Performance and Cathode Coupling Voltage," *43rd AIAA/ASME/SAE/ASEE Joint Propulsion Conference & Exhibit*, NASA, 2007.

[6] Morozov A. I. and Savelyev V. V., "Fundamentals of Stationary Plasma Thruster Theory," *Reviews of Plasma Physics*, Vol.21, 2000, pp: 203, 382.

[7] Sekerak, M., et al, "Hall Thruster Plume Measurements from High-speed Dual Langmuir Probes with Ion Saturation Reference," *IEEE Aerospace Conference*, IEEEE, 2013.

[8] Sommerville, J. D. and King, L. B., "Hall-effect Thruster-cathode Coupling, Part II: Ion Beam and Near-field Plume," *Journal of Propulsion and Power*, Vol.27, No.4, 2011, pp: 754, 767.

[9] Khartov, S., Nazarenko, I., Pereslavtsev, A., "Plasma Parameters Investigation in the Near Cathode Zone of the SPT Discharge," *30th International Electric Propulsion Conference*, 2007.

[10] Knoll, A. K., Thomas, N., Gascon, N., Cappelli, M., "Experimental Investigation of High Frequency Plasma Oscillations within Hall Thrusters," *42nd Joint Propulsion Conference＆Exhibit*, NASA, 2006.

[11] Smith, A. W. and Cappelli, M. A., "Time and Space-correlated Plasma Potential Measurements in the Near Field of a Coaxial Hall Plasma Discharge," *Physics of Plasmas*, Vol.16, No.7, 2009.

[12] Dannenmayer, K., Mazouffre, S., Kudrna, P., and Tichý, M., "The Time-Varying Electron Energy Distribution Function in the Plume of a Hall Thruster," *Plasma Sources Science and Technology*, Vol.23, No.6, 2014.

[13] Xu, K. G., and Walker, M. L., "Effect of External Cathode Azimuthal Position on Hall-Effect Thruster Plume and Diagnostics," *Journal of Propulsion and Power*, Vol.30, No.2, 2014, pp: 506, 513.

[14] Albarede, L., Vial, V., Lazurenko, A., Bouchoule, A., Dudeck, M., "Hollow Cathode Stationary and Dynamical Behavior: in Diode Regime and with a Hall Thruster" *4th International Spacecraft Propulsion Conference*, ESA, 2004.

[15] Mikellides, I. G., Jongeward, G. A., Katz, I., et al., "Plume Modeling of Stationary Plasma Thrusters and Interactions with the Express-A Spacecraft," *Journal of Spacecraft and Rockets*, Vo.39, No.6, 2002, pp: 894, 903.

[16] Ortega, A. L., Mikellides, I. G., "The Importance of the Cathode Plume and its Interactions with the Ion Beam in Numerical Simulations of Hall Thrusters," *Physics Of Plasmas*, 2016, Vol.23, No.4, 2016.

[17] Ortega, A. L., Katz, I., Mikellides, I. G., et al., "Self-Consistent Model of a High-Power Hall Thruster Plume," *IEEE Transactions on Plasma Science*, 2015, Vol.43, No.9, 2015, pp: 2875, 2886.

[18] Frieman, J. D., Walker, J. A., Walker, M. L. R., Khayms, V., King, D. Q., "Electrical Facility Effects on Hall Thruster Cathode Coupling: Performance and Plume Properties," *Journal of Propulsion and Power*, Vol. 32, No. 1, 2015.

[19] Yu, D., Meng, T., Ning, Z., Liu, H., "Confinement Effect of Cylindrical-separatrix Type Magnetic Field on the Plume of Magnetic Focusing Type Hall Thruster," *Plasma Sources Science and Technology*, Vol.26, No.4, 2017.

[20] UNAM database, www.lxcat.net, retrieved on September 14, 2017.